Effect of Y addition and cooling rate on refinement of eutectic Si in Al–5 wt-%Si alloys

J. H. Li*[1] and P. Schumacher[1,2]

A series of Al–5 wt-%Si alloys with or without 200 ppm Y addition have been produced using conventional casting and melt spinning respectively. The effects of Y addition and cooling rates on the refinement of eutectic Si have been investigated using thermal analysis, differential scanning calorimetry and multiscale microstructure characterisation techniques. In the case of conventional casting, the addition of up to 200 ppm Y was found to cause no modification effect. The eutectic Si presented a plate-like structure rather than a fibrous morphology. No significant Si twinning was observed. In the case of melt spinning, a higher cooling rate caused a much finer eutectic Si and Si twinning. The addition of 200 ppm Y promoted heavier multiply Si twinning. After a continuous cooling from 873 to 673 K, an Al_2SiY phase was observed beside or within the Si particle. The refinement mechanism was also discussed.

Keywords: Al–Si alloy, Y additions, Refinement, Eutectic solidification, TEM

Introduction

Al–Si based alloys, i.e. A356, are dominant in foundry application, which constitutes the majority of all castings. The size and shape of eutectic Si in hypoeutectic Al–Si alloys and of primary Si in hypereutectic Al–Si alloys have a great effect on the final mechanical properties of the manufactured parts. The modification of the Si morphology from flake-like to fibrous form was believed to greatly improve the mechanical properties. Therefore, the modification of eutectic Si in Al–Si alloys has been widely investigated since the first modification phenomenon was discovered by Pacz in 1920,[1] where an Al–15 wt-%Si alloy was stirred in a sodium fluoride flux and a remarkable increase in the mechanical properties was achieved. The modification of the eutectic Si in hypoeutectic Al–Si alloys is normally achieved in two different ways: by addition of certain modified elements (chemical modification)[2–13] or by rapid solidification (quench modification),[13] although ultrasonic vibration[14] and electromagnetic field[15] were also reported to refine the eutectic Si.

In the aspect of chemical modification, several common modifying elements, i.e. Sr, Na and Sb, have been widely investigated over the years and are widely used in the casting industry to modify the Si morphology from flake-like to fine fibrous. Apart from the common modified elements (i.e. Sr, Na and Sb), the rare element (i.e. Y) was also reported to refine the eutectic Si at a relatively higher content.[4,5] However, to date, there is still a lack of detailed investigation on the effect of Y on the eutectic Si phase in Al–Si alloy, although very limited previous reports are available in the literature.[4,5] Special pertinent questions that remain to be explored are the distribution of Y at the reentrant edges/or corner of the Si crystal and the effect of Y on Si twinning. A better understanding on the refinement of eutectic Si caused by the Y addition is of great importance to further improve the mechanical properties. Thus, one main motivation of this study is to investigate the effect of Y addition on the eutectic Si phase in Al–5 wt-%Si alloys, with a focus on the distribution of Y and Si twinning.

In the aspect of quench modification, our recent melt spun experiments on Al–5 wt-%Si alloys with and/or without trace modified elements (Sr and P) clearly reveal that nanoscale faceted twinned Si particles were formed directly from the liquid.[13] The precipitation of Si from supersaturated solid solution in the α-Al matrix during subsequent cooling was also greatly enhanced in these melt spun Al–Si based alloys. The finer microstructure and the enhanced hardening effects produce better mechanical properties. However, the effect of Y addition on the nucleation and growth of eutectic Si in melt spun Al–Si alloy remains to be explored. On the other hand, a higher cooling rate (10^6 K s^{-1}, melt spinning) can extend the solid solubility of Y in the α-Al matrix.[16] The higher solid solubility of Y in Al or Si can be expected to result in a redistribution of the Y element and thus Si twinning. A further research on the effect of higher cooling rates (i.e. melt spinning) is also required. Thus, another main motivation of this study is to elucidate the effect of cooling rates on the refinement or modification of eutectic Si in Al–Si based alloys.

Experimental

A series of high purity Al–5 wt-%Si alloys (wt-% was used throughout the paper unless otherwise noted) with

[1]Department of Metallurgy, The University of Leoben, Leoben A-8700, Austria
[2]Austrian Foundry Research Institute, Parkstrasse 21, Leoben, Styria A-8700, Austria

*Corresponding author, email jie-hua.li@hotmail.com

Received 31 January 2012; accepted 12 September 2012
DOI 10.1179/1743133612Y.0000000039

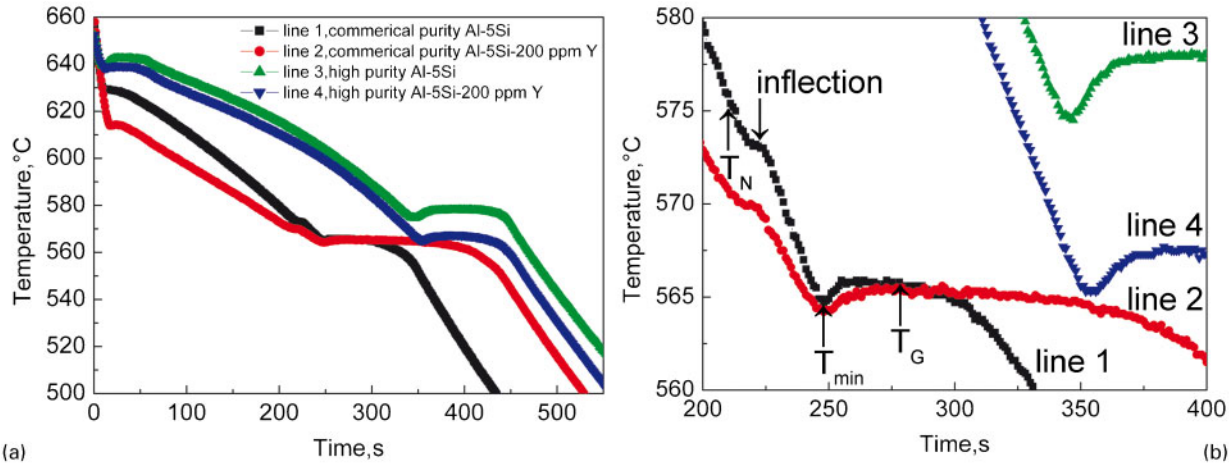

1 ***a*** **cooling curves taken from Al–5Si alloys with and without 200 ppm Y addition and** ***b*** **eutectic arrest area is enlarged and main points (T_N, T_{min} and T_G) are also marked**

and without 200 ppm Y addition were prepared using conventional casting and melt spinning respectively. For conventional casting, high purity Al–5Si (alloy C) and Al–5Si–200 ppm Y (alloy D) alloys were prepared using Al (4N, means 99·99%, the same as below), Si (5N) and Al–3·4Y master alloy. For comparison, commercial purity Al–5Si (alloy A) and Al–5Si–200 ppm Y (alloy B) alloys were also prepared using commercial purity Al (99·7), Al–12Si (containing 0·9Fe and 0·355Mn) master alloy and Al–3·4Y master alloy. These alloys were melted in an electric resistance furnace, and the temperature of the melt was kept at 993 K. The Al–3·4Y master alloy was added before the casting. No degassing was performed before the casting. About 5 min after the Al–3·4Y master alloy was added, thermal analysis was performed to elucidate the thermal kinetics during solidification. At least two samples for each addition level were taken to perform thermal analysis using a quick cup method.

Samples for optical microscopy were taken from the centre parts (about half height), where the thermal couple was located and the cooling condition was measured. The specimens were mechanically ground, polished and then etched using a mixture of 13 g boric acid, 35 g HF and 800 mL H_2O. Samples for TEM observation were prepared using the same method as melt spun ribbons, as described later.

For melt spinning, as described elsewhere,[13] high purity materials (4N Al, 5N Si and 3N Y) were used to produce Al–5Si (alloy E) and Al–5Si–200 ppm Y (alloy F). It is noteworthy that the Y contents (200 ppm in alloys B, D and F) were added with an Al–3·4Y master alloy manufactured by 4N Al and 3N Y. The chemical compositions of the experimental alloys were determined by inductively coupled plasma atomic emission spectrum apparatus and are given in Table 1.

For alloys E and F, the ribbons were investigated in the as melt spun condition and after heating to 873 K and subsequent continuous cooling in the range from 873 to 673 K with a rate of 10 and 1 K min^{-1} respectively, in a power compensated differential scanning calorimetry (DSC; PerkinElmer Diamond), with the aim to investigate the microstructure evolution depending on the thermal history. The thermal response during cooling is the subject of this paper. The ribbons for TEM investigation were mechanically ground, polished and dimpled to ~30 μm and then ion beam milled using a Gatan precision ion polishing system (Gatan model 691). A constant preparation temperature (~263 K) was maintained using a cold stage during ion beam polishing. Transmission electron microscopy was performed using a Philips CM12 microscopy operated at 120 kV equipped with a charge coupled device camera (Gatan model 794 MSC BioScan).

Results

Thermal analysis of Al–5Si alloys with and without 200 ppm Y addition

Figure 1 shows typical cooling curves taken from Al–5Si alloys with and without 200 ppm Y addition. The eutectic arrest area was also enlarged in Fig. 1*b*. The cooling rate during thermal analysis was evaluated to be ~22 K min^{-1}. The main points (eutectic nucleation temperature T_N, minimum temperature T_{min} and growth temperature T_G) were determined and are listed in Table 2. It is worth noting that T_N is defined to be the temperature when the Si crystals nucleate and grow. It was extracted from the cooling curve and corresponding derivative curve (dT/dt, not shown here) where two slope tangents cross.[4] The minimum temperature T_{min} is defined as the point where the newly nucleated crystals, together with aluminium in the eutectic proportions, have grown to such an extent that the latent heat, evolved during the growth process, balances the heat flow out of the system. This depends upon the cooling rate and heat capacity of the solidifying system. After this point, recalescence occurs, during which the release of latent heat surmounts the heat extraction from the system, and a new heat balance is obtained, which

Table 1 Chemical compositions of Al–5Si alloys with and without 200 ppm Y addition/wt-%

	Elements				
Alloys	Si	Fe	Mn	Y/ppm	Al
Alloy A (casting)	5·00	0·37	0·11	…	Balance
Alloy B (casting)	5·00	0·37	0·11	200	Balance
Alloy C (casting)	5·00	…	…	…	Balance
Alloy D (casting)	5·00	…	…	200	Balance
Alloy E (melt spun)	5·00	…	…	…	Balance
Alloy F (melt spun)	5·00	…	…	200	Balance

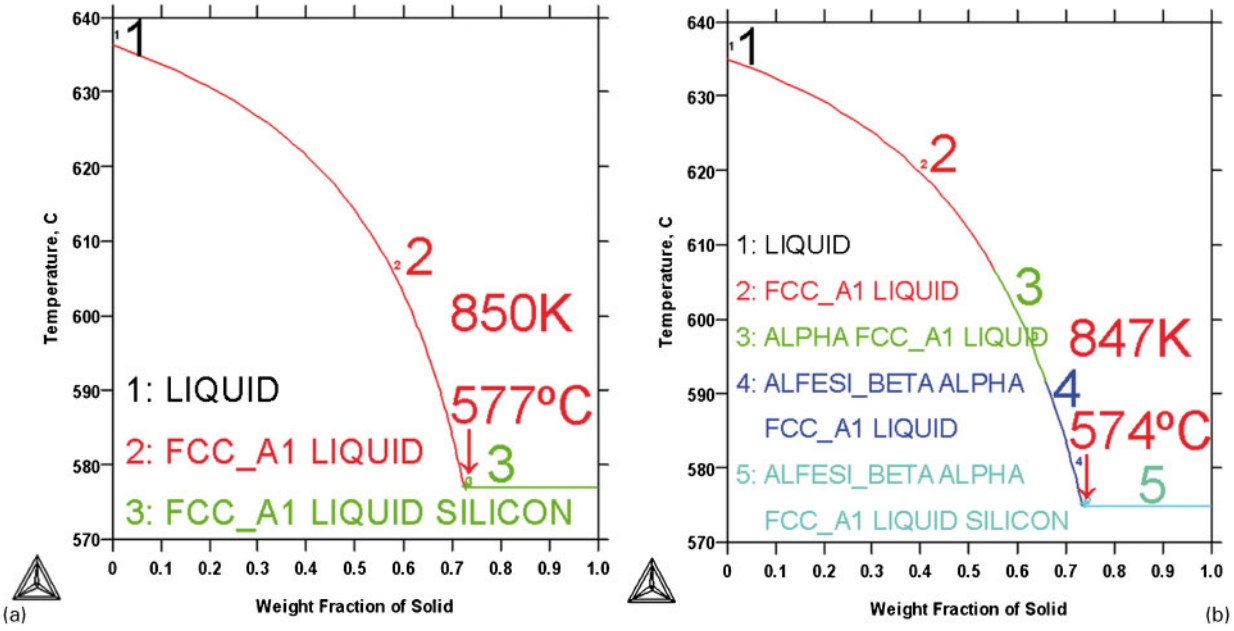

2 Weight fraction of phases in commercial purity Al–5Si alloy *a* without and *b* with Fe (0·37) and Mn (0·11) impurities, simulated using Scheil module with database TTAL5

rightfully should be defined as the 'steady state growth temperature' of the eutectic reaction. Recalescence is the difference between the T_{min} and T_G temperatures (T_G–T_{min}).

The measured T_N (i.e. 847 K for alloy A without Y addition) is close to the predicted equilibrium eutectic temperature (847 K) using ThermoCalc Scheil simulation with TTAL5 database, as shown in Fig. 2*b*. It should be noted that the nucleation temperature T_N is affected by the nucleation conditions in the alloys and is also related to the nucleation undercooling. ThermoCalc Scheil simulation cannot handle this issue. However, ThermoCalc Scheil simulation indicates that the impurity elements (Fe and Mn) depress the equilibrium eutectic temperature from 850 to 847 K, as shown in Fig. 2*a*. The predicted eutectic temperature (850 K) was defined to be the equilibrium eutectic temperature T_{eq} in Al–5Si alloy.

Up to 200 ppm Y addition into commercial purity Al–5Si alloy (alloy B) results in the eutectic nucleation temperature T_N displaced to a lower temperature (from 847 to 844·8 K). The eutectic growth temperature T_G was also displaced to a lower temperature (from 838·6 to 838·4 K). In the case of high purity Al–5Si alloys (alloys C and D), a slight higher eutectic nucleation temperature (1·5 and 0·3 K, compared with the commercial purity Al–5Si and Al–5Si–200 ppm Y respectively) was observed. The measured T_N (i.e. 865·1 K for alloy D) is in good agreement with the measured eutectic Si nucleation temperature (865·9 K) using DSC, as shown in Fig. 3*b*. However, the eutectic Si nucleation temperature cannot be obtained from DSC in commercial purity Al–5Si–200 ppm Y (alloy B) because of the nucleation of β-Al_5FeSi phase at 863·48 K (Fig. 3*a*). The addition of 200 ppm Y into high purity Al–5Si alloy (alloy D) also results in eutectic growth temperature decreases from 850·9 to 840·5 K. It is worth noting that an inflection was observed for commercial purity alloys (alloys A and B), as marked with a black arrow in Fig. 1*b*, while no similar inflection was observed for high purity alloys (alloys C and D). The presence of the inflection may be attributed to the impurity effects of Fe and Mn elements on the nucleation and growth of eutectic Si, i.e. the formation of β-Al_5FeSi phase, as predicted in Fig. 2*b*.

The nucleation undercooling ($T_{eq}-T_N$) of the eutectic arrest was determined. A small undercooling (3·0 K for alloy A and 1·5 K for alloy C) was observed. The addition of 200 ppm Y results in an increasing undercooling, i.e. 5·2 K for alloy B and 4·9 K for alloy D. The increase in undercooling can be attributed to the decrease in possible nucleus (i.e. AlP) poisoned by the Y addition and the formation of Al_2SiY phase, as discussed later.

The recalescence (T_G-T_{min}) of the eutectic arrest was also determined. A small recalescence (1·1 K for alloy A and 1·2 K for alloy B) was observed in commercial purity Al–5Si alloys. This small recalescence may be due to the impurity effect of Fe and Mn. A slight higher recalescence (3·4 K for alloy C and 2·2 K for alloy D)

Table 2 Nucleation T_N, minimum T_{min}, growth temperature T_G, nucleation undercooling and eutectic recalescence for Al–5Si alloys with and without 200 ppm Y addition

Alloys	Y/ppm	T_N/K	T_{min}/K	T_G/K	Nucleation undercooling $T_{eq}-T_N$/K	Recalescence T_G-T_{min}/K
Alloy A	…	847·0	837·5	838·6	3·0	1·1
Alloy B	200	844·8	837·2	838·4	5·2	1·2
Alloy C	…	847·5	847·5	850·9	3·5	3·4
Alloy D	200	845·1	838·3	840·5	4·9	2·2

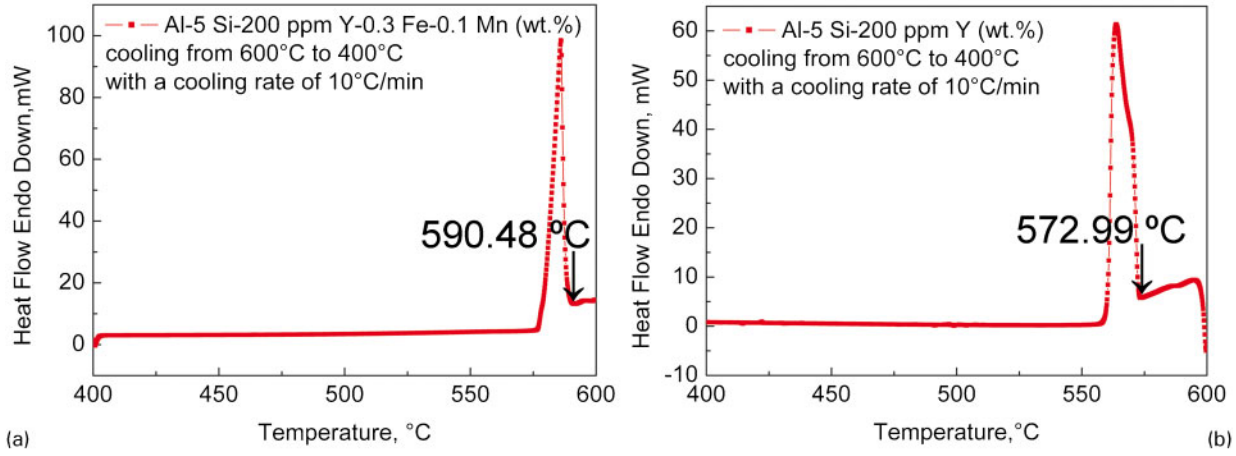

a commercial purity Al–5Si–200 ppm Y alloy; *b* high purity Al–5Si–200 ppm Y alloy

3 Differential scanning calorimetry curves of Al–5Si alloys with 200 ppm Y addition: cooling rate is 10 K min^{-1}

before the eutectic growth was observed in high purity Al–5Si alloys. Clearly, the 200 ppm Y addition does not cause a significant increase in recalescence.

Optical microscopy of Al–5Si alloys with and without 200 ppm Y addition

Figure 4 shows representative eutectic Si structures of Al–5Si alloys with and without 200 ppm Y addition after conventional casting, observed by optical microscopy at a low magnification. The eutectic Si in alloy A without Y addition is very coarse and flake-like. With the addition of up to 2000 ppm Y (alloy B), the eutectic Si structure remains unchanged. The eutectic Si is still plate-like, although a decrease in Si size was observed. The addition of high purity elements (alloys C and D) causes a refined plate-like structure, although no significant difference, i.e. recalescence (2·2 K for alloy D), was observed during thermal analysis (Fig. 1 and Table 2).

Figure 5 shows representative eutectic Si structures of Al–5Si alloys with and without 200 ppm Y addition after melt spinning, observed by optical microscopy at a lower magnification and by SEM at a higher magnification. A higher cooling rate greatly refines the Si, as compared with Fig. 4. However, up to 200 ppm Y addition does not greatly refine eutectic Si (Fig. 5). Two kinds of Si particles were observed. One is distributed along the grain boundaries. The other is entrained within the α-Al matrix (eutectic droplet). Energy dispersive X-ray (EDX) analysis (Fig. 5*d*) of the eutectic droplet, as marked with a white arrow in Fig. 5*c*, indicates that it contains ~52 at-%Al and 48 at-%Si. This observation is also fully consistent with the DSC analysis.

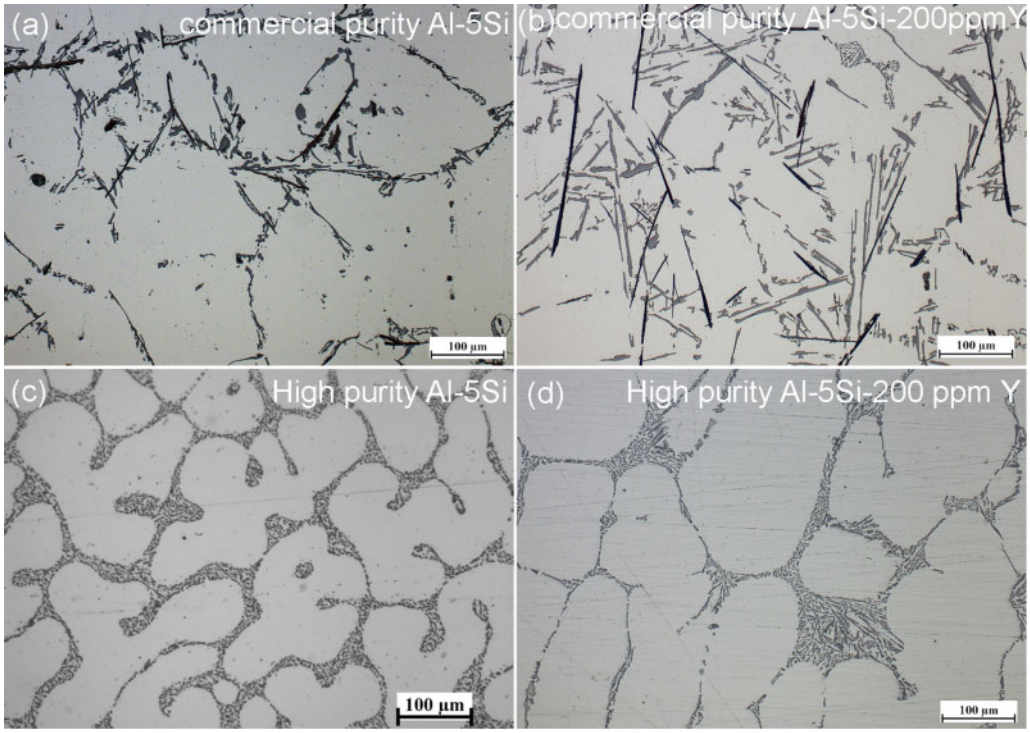

a commercial purity Al–5Si alloy; *b* commercial purity Al–5Si–200 ppm Y alloy; *c* high purity Al–5Si alloy; *d* high purity Al–5Si–200 ppm Y alloy

4 Representative eutectic structures observed by optical microscopy at low magnification

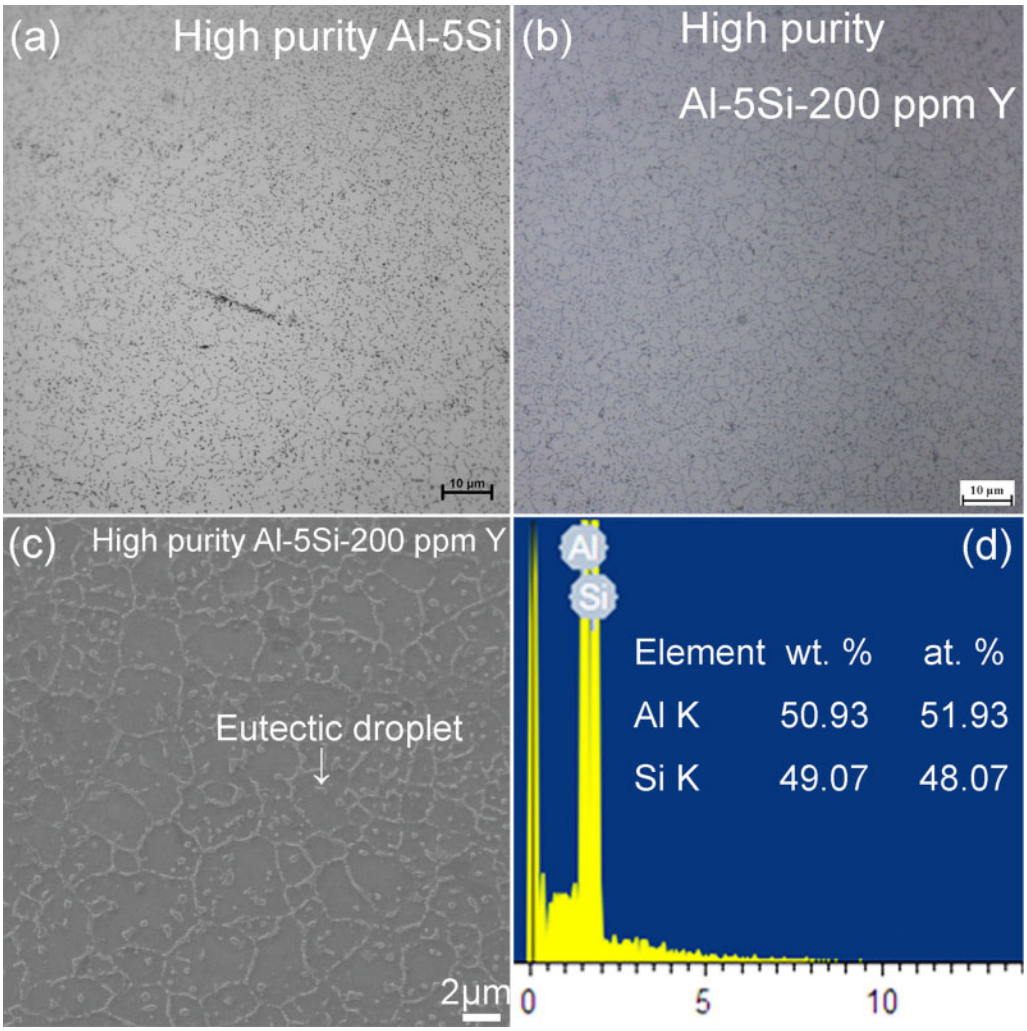

a high purity melt spun Al–5Si alloy; *b*, *c* high purity melt spun Al–5Si–200 ppm Y alloy; *d* EDX analysis of eutectic droplet as marked with white arrow in *c*

5 Representative structures observed by optical microscopy at low magnification and by SEM at higher magnification

Differential scanning calorimetry analysis of high purity melt spun Al–5 wt-%Si alloys with and without 200 ppm Y addition

Figure 6 shows the DSC curves of high purity melt spun Al–5Si alloys with and without 200 ppm Y addition at two different cooling rates (10 and 1 K min^{-1} respectively). In the case of Al–5Si without 200 ppm Y addition, the first sharp exotherm A occurs with an onset temperature of 848·13 K, which is 1·87 K less than the equilibrium eutectic temperature (850 K), as shown in Fig. 2*a*, while the small exotherm B occurs with an onset temperature of 827·07 K. As suggested by Cantor and co-workers,[17] exotherm A represents the solidification of eutectic Si along the grain boundary, while exotherm B represents the solidification of entrained eutectic Si (droplet) within the α-Al matrix. Undercooling can be measured by a difference between the onset temperatures of the grain boundary eutectic peak and droplet peak. In the case of Al–5Si, the undercooling ΔT was measured to be ~21·06 K.

In the case of Al–5Si with 200 ppm Y addition, the first sharp exotherm A occurs with an onset temperature of 847·80 K, which is 2·20 K less than the equilibrium eutectic temperature. The small exotherm B occurs with an onset temperature of 826·12 K. The undercooling ΔT was measured to be ~21·68 K. Clearly, no great effect of 200 ppm Y addition on undercooling was observed. This is also consistent with the thermal analysis during conventional casting (Fig. 1 and Table 2).

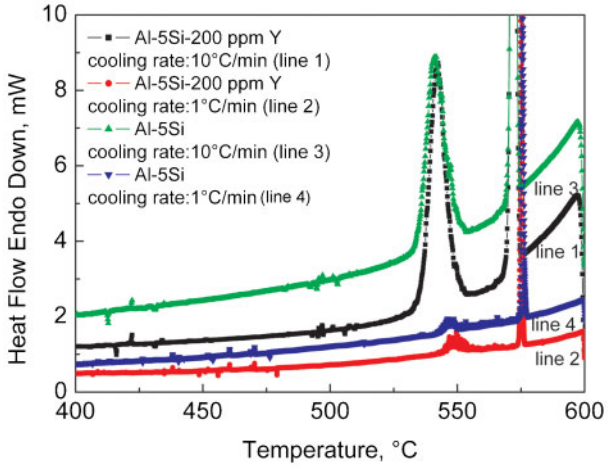

6 Differential scanning calorimetry curves of high purity melt spun Al–5Si alloys with and without 200 ppm Y addition: cooling rates are 10 and 1 K min^{-1} respectively

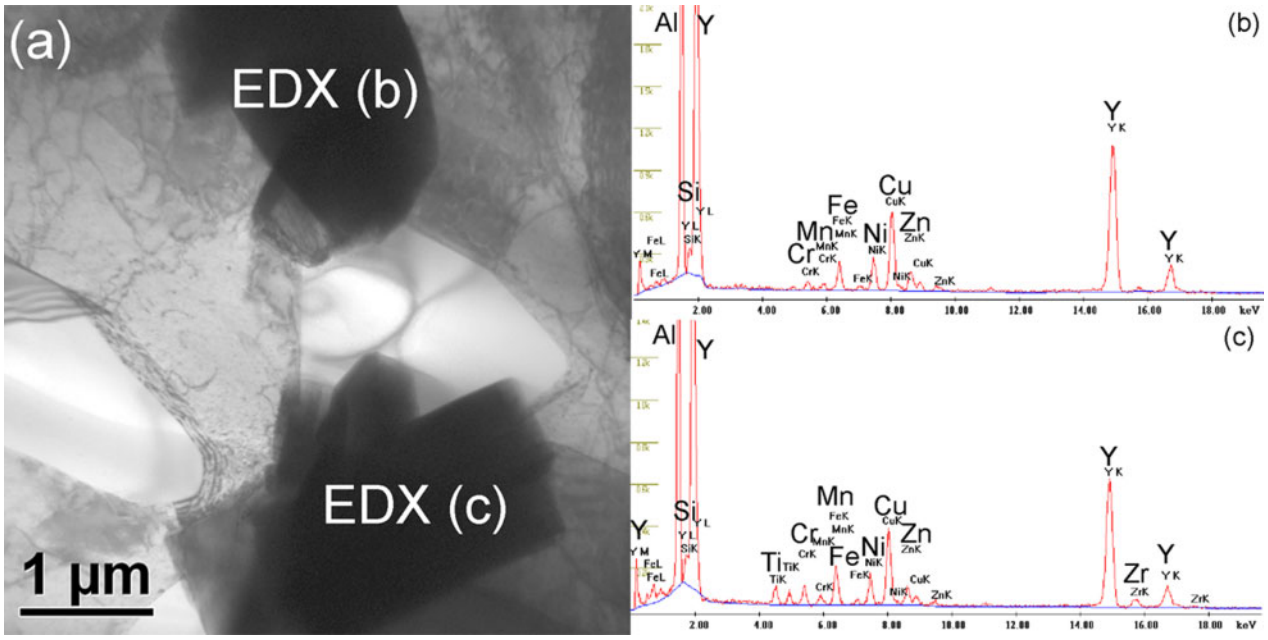

7 ***a*** **bright field image (TEM) and** ***b***, ***c*** **corresponding EDX analyses of Y containing particles in commercial purity Al–5Si–200 ppm Y alloy**

Transmission electron microscopy observation of Al–5Si alloys with and without 200 ppm Y addition

Figure 7 shows the TEM bright field image and the corresponding EDX analyses of the Y containing particles in commercial purity Al–5Si–200 ppm Y alloy (alloy B) produced by conventional casting. Both two particles (EDX b and c) seem to be an AlY phase according to their composition analyses. [The ratio of Al and Y is ~1 : 1, although other elements (i.e. Si, Cu, etc.) are also measured.] The formation of AlY particles may be attributed to the enrichment of solute Y during solidification. However, no similar AlY phase was observed in the high purity melt spun Al–5Si–200 ppm Y alloy, possibly due to the higher solubility of Y caused by higher cooling rates. The AlY phase (cubic, a=0·375 nm, Table 3)[18] was not expected to be a good nucleating site for Si, although some Si particles seem to be associated with these AlY phases. The Si particles were tilted to the principal twinning orientation of Si (<110>). However, unexpectedly, no significant Si twin was observed.

Figure 8 shows the TEM bright field image and the corresponding selected area diffraction pattern (SADP) of a droplet within the α-Al matrix in high purity melt spun Al–5Si–200 ppm Y alloy. The size of the droplet is ~3 μm. Within the droplet, Si particles are randomly distributed. The size of these Si particles varies from 0·1 to 0·2 μm. The smaller size of Si particles within the droplets may suggest the nucleation environment is uniform. A homogeneous nucleation can be expected. The measured undercooling (Fig. 6) can be attributed to the sole effect of the alloying element (i.e. Y).

Figure 9 shows a Si particle in high purity melt spun Al–5Si alloy with 200 ppm Y addition. The Si particle was tilted to the principal twinning orientation of Si (<110>) to observe the Si twin. In contrast to alloy D produced by conventional casting (a much lower cooling rate), most Si particles were multiply twinned. It should be noted that similar twinned Si particles were also observed in high purity melt spun Al–5Si alloy without 200 ppm Y addition; however, most of the Si twinning was along only one special direction rather than multiple directions.[13] The corresponding SADP (Fig. 9*b*) indicates that the Si twin grows along the $\{111\}_{Si}$ plane. The angle between the two different twinning planes is close to 70·5°. The faceted morphology of the twinned Si particle can be understood in terms of the interface energies between Si and Al.

After continuous controlled cooling, the size of these Si particles increases, while their amount decreases. A few large Si particles were observed on grain boundaries. Figure 10 shows a Si particle on the grain boundary in high purity melt spun Al–5Si–200 ppm Y alloy after continuous cooling in the range from 873 to 673 K with a cooling rate of 10 K min^{-1}. The corresponding SADP (Fig. 10*c*) and the centred dark field image (Fig. 10*b*) using the diffraction spot as marked in Fig. 10*c* indicate

Table 3 Crystallographic data for some selected phases

No.	Phase	Crystal structure	Lattice parameter/nm	Disregistry δ/%
1	Al	Cubic	a=0·40491	25 when $(Al)_{Substrate}$
2	Si	Cubic	a=0·5421	…
3	Al_2Si_2Sr	Hexagonal	a=0·4187, c=0·7427	23 when $(Al_2Si_2Sr)_S$
4	Al_2SiY	…	…	…
5	AlY	Cubic	a=0·375	>25 when $(AlY)_{Substrate}$
6	AlP	Cubic	a=0·5431	<1 when $(AlP)_S$
7	YP	Cubic	a=0·5661	<1 when $(YP)_S$

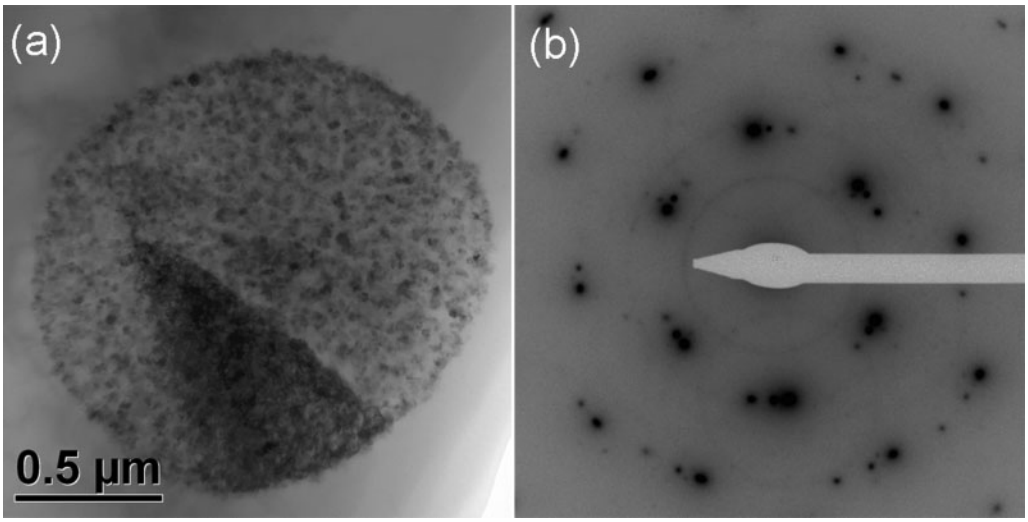

8 ***a*** **bright field image (TEM) and** ***b*** **corresponding SADP of eutectic droplet within** α**-Al matrix in high purity melt spun Al–5Si–200 ppm Y alloy**

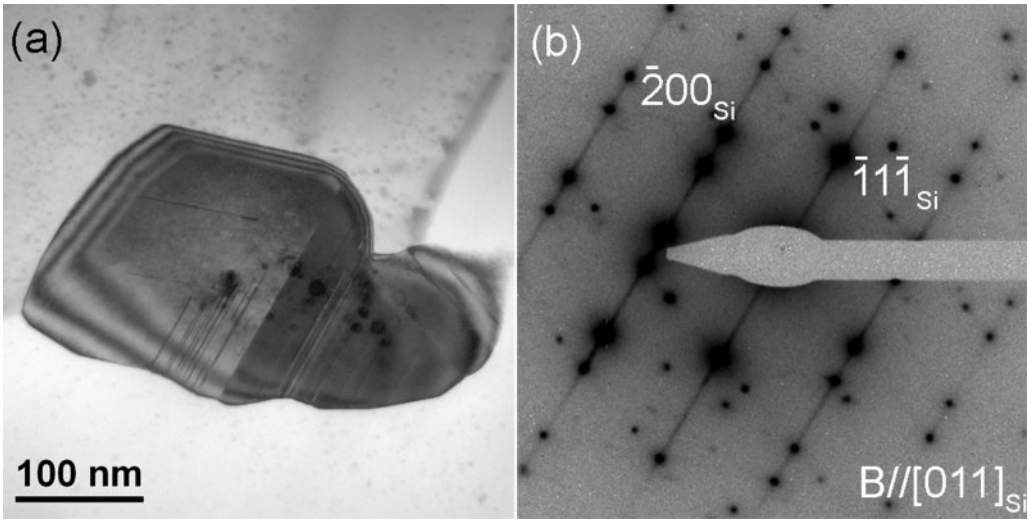

9 ***a*** **bright field image (TEM) and** ***b*** **corresponding SADP of Si twinning on grain boundary in high purity melt spun Al–5Si–200 ppm Y alloy**

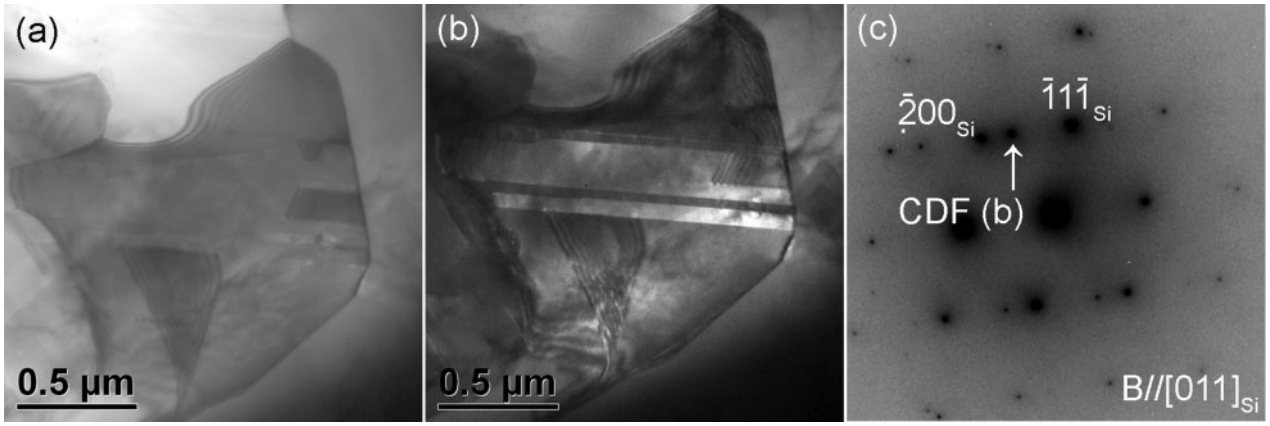

10 ***a*** **bright field image (TEM),** ***b*** **centred dark field image and** ***c*** **corresponding SADP of Si twinning on grain boundary in high purity Al–5Si–200 ppm Y alloy after continuous cooling in DSC from 873 to 673 K with cooling rate of 10 K min^{-1}**

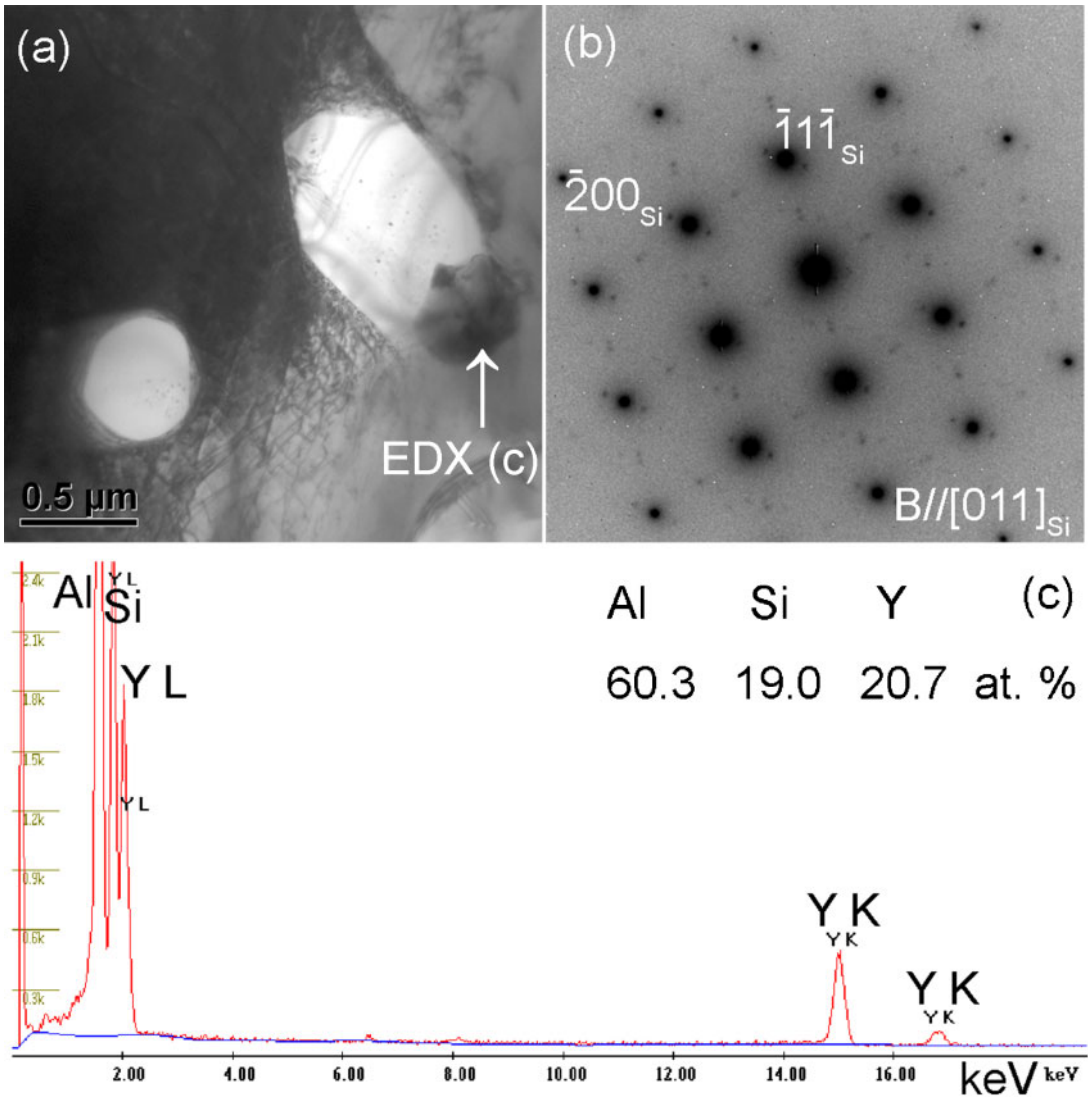

11 ***a*** **bright field image (TEM),** ***b*** **corresponding SADP and** ***c*** **EDX analysis of Y containing particle in high purity melt spun Al–5Si–200 ppm Y alloy after continuous cooling in DSC from 873 to 673 K with cooling rate of 10 K min^{-1}**

again that the Si twin grows along the $\{111\}_{Si}$ plane. Fewer twins, i.e. lower twin densities, were observed as compared to the as melt spun condition (Fig. 9*a*). The size of the Si particles after continuous cooling was found to be about 1·5–3 μm in length and 1–2 μm in width. It is much larger than that (~200 nm) in the as melt spun condition, as shown in Fig. 9*a*. Clearly, a ripening process occurs during the continuous cooling from 873 to 673 K with a cooling rate of 10 K min^{-1}.

Apart from the Si particle, another Y containing phase was also observed in the high purity melt spun Al–5Si–200 ppm Y alloy after continuous cooling in the range from 873 to 673 K with a cooling rate of 10 K min^{-1}, as shown in Fig. 11*a*. Energy dispersive X-ray analysis (Fig. 11*c*) of the Y containing phase, as marked with a white arrow in Fig. 11*a*, indicates that this Y containing phase seems to be Al_2SiY phase. The higher Al content can be attributed to the small size (~400 nm) of the Al_2SiY phase and the large beam size (~100 nm) used for EDX measurement. Another long plate-like Y containing phase was also observed within the Si particle, as shown in Fig. 12*a*. Energy dispersive X-ray analysis (Fig. 12*b*) of the Y containing phase, as marked in Fig. 12*a*, also indicates that this Y containing phase seems to be Al_2SiY phase. However, Y atoms do not concentrate in the eutectic Si (Fig. 12*c*) within the limitation of the detected resolution (EDX).

Discussion

Formation of Al_2SiY or YP phases

Y was mainly consumed though the formation of the Al_2SiY phase (Figs. 11 and 12) or the YP phase (not observed here). The formation of Al_2SiY phases in the Al–Si–Y alloy (alloy F) is different from the formation of Al_2Si_2Sr phase in the Al–Si–Sr alloy[13] partly due to the lower Y addition (200 ppm) and lower Y solubility [0·17 wt-% (0·05 at-%) at 1185 K].[19] It can be expected that the formation of Al_2SiY phase deteriorates the effect of Y additions on eutectic Si. Although the crystallographic data of Al_2SiY phase are not available, it can be expected that the Al_2SiY phase is not a nucleation site for eutectic silicon in hypoeutectic Al–Si alloys, similar to Al_2Si_2Sr phases, as shown in Table 3.

On the other hand, the formation of YP phase may also reduce the amount of potent AlP phase. The AlP phase is believed to be responsible for the Si nucleation in both hypo- and hypereutectic Al–Si alloys, as its

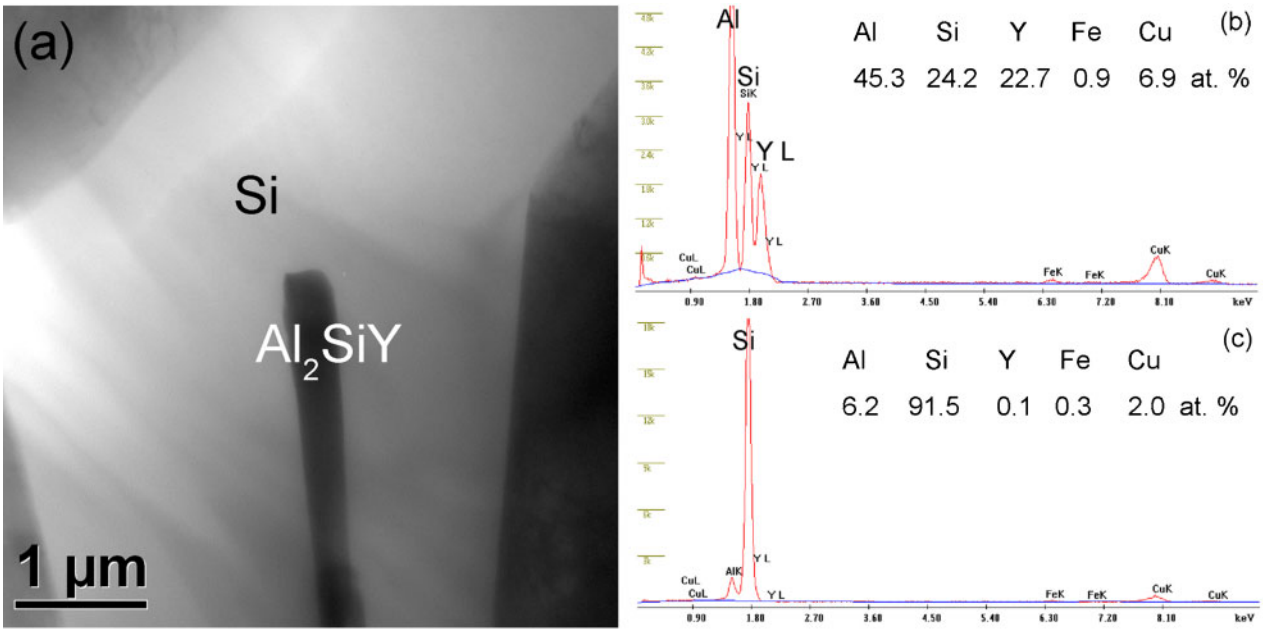

12 ***a*** **bright field image (TEM) and** ***b***, ***c*** **corresponding EDX analyses of plate shaped Si phase and Al_2SiY phase in high purity melt spun Al–5Si–200 ppm Y alloy after continuous cooling in DSC from 873 to 673 K with cooling rate of 10 K min^{-1}**

crystal structure and lattice parameter have an excellent match with Si (Table 3). The lattice parameters for AlP and Si are 0·542 and 0·54306 nm, and the corresponding structure types are B_3 and A4 respectively.[20] The disregistry between AlP and Si is only <1%, as calculated by an equation proposed by Turnbull and Vonnegut.[21] Although the crystal structure and lattice parameter of YP phase (Fm3m, NaCl, a=0·5661 nm)[20] are very close to that of the AlP, the potency for Si nucleation is not yet experimentally supported. We believe a size effect may play an important role despite the similar lattice parameter of both AlP and YP phases. AlP is expected to be adsorpted in relative large patches on Al to reduce the required free growth energy, while YP may be presented unfavourably as small patches on Al or as small YP patches. The possible poisoning effect of Y on AlP forces the nucleation of silicon at lager undercoolings (Fig. 1).

Although there is a lack of strong experimental support to the existence of YP phase in this present study considering the expected level of P (<20 ppm), the possible existence of YP phase can be strongly supported in terms of thermodynamics (enthalpy and Gibbs energy) of competing phosphide compounds (i.e. Na_3P, Sr_3P_2 and YP). As listed in Table 4, the free enthalpy ΔG (as documented by Schlesinger)[22] of the YP phase is −344 kJ mol^{-1}, much lower than that of AlP (−111·66 kJ mol^{-1}). It should be noted that the free enthalpy ΔG of other phosphide compounds (i.e. FeP, CrP and MnP) is much closer to the value of AlP, which is consistent with the fact that these elements have no great influence on the nucleation of eutectic Si in Al–Si alloys. The thermodynamic consideration strongly supports that the YP phase is thermodynamically more stable and is highly likely to be preferentially formed, even AlP acting as a nucleation site for Si. This also strongly supports the hypothesis that the formation of the YP phase will consume P and force the nucleation of Si to a higher undercooling, as observed in Table 2.

Table 4 Enthalpy and entropy values for different phosphides

Phosphide compounds	Enthalpy ΔH^{o}_{298}/kJ mol^{-1}	Entropy ΔS^{o}_{298}/J mol^{-1} K^{-1}
AlP	−111·66	57·3
SiP	−38·84	40·30
Ca_3P_2	−506	55·30
Sr_3P_2	−635	…
Na_3P	−134	…
ScP	−344	51
LaP	−363·72	66·82
YP	−344	70

The formation of the YP phase is also consistent with the formation of other P containing phases, i.e. the formation of Na_3P (Ref. 23) in the case of Na addition, and the formation of Sr_3P_2 compound in the case of Sr addition.[13,24] In both cases of Na and Sr, the estimated free enthalpy of the formation of Na_3P and Sr_3P_2 (−635 and −134 kJ mol^{-1} respectively) is much less than that of the AlP phase (−-111·66 kJ mol^{-1}).[22,25] The same hypothesis may be also true with the addition of Sc, La and Ca elements, having even more negative ΔG, as listed in Table 4. With the presence of elements with a smaller enthalpy ΔG, the AlP will deplete the nucleation sites for Si. The remaining amount of AlP will be determined by the competing phosphides, which were only reported in some cases.[23] It is important to point out that the lack of AlP only results in an increased nucleation undercooling and thereby a refinement of the eutectic Si structure but cannot explain the modification caused by Si twinning.

Effect of cooling rate on refinement of eutectic Si

No significant Si twinning was observed in commercial purity Al–5Si–200 ppm Y alloy (Fig. 7) after conventional casting. This is in contrast to the prediction of the

impurity induced twinning (IIT) growth mechanism proposed by Lu and Hellawell[2] and the twin plane re-entrant edge growth mechanism (TPRE) proposed by Wanger[26] and Hamilton and Seidensticker.[27] The TPRE growth mechanism proposed that growth occurred more readily at the re-entrant corners, which could play a role in the modification of Ge crystals. The IIT growth mechanism proposed that the impurities were adsorbed on the growing surfaces of Si and caused frequent twinning to occur. The geometrical/ideal radius ratio $r_{modifier}/r_{Si}$ to cause IIT is ~1·646. Both IIT and TPRE mechanisms have been experimentally supported in the case of Sr[9,13] and Eu.[11] The segregation of Sr and Eu into eutectic Si indeed causes a fine fibrous morphology. However, no similar experimental support was observed in the case of Y (Fig. 7), even though Y has a suitable radius ratio of r_Y/r_{Si}=1·459, also fitting the IIT theory.

Apart from the atomic radius ratio $r_{modifier}/r_{Si}$, another effective parameter (i.e. mixing enthalpy) for the selection of the modifying agent for Al–Si was also suggested.[28] As suggested in Ref. 28, Y has a large negative mixing enthalpy with Si. The addition of 3 wt-%Y into the Al–14Si alloy was also found to modify the eutectic Si. However, in present study, no significant modification effect was observed in alloys B and D produced by conventional casting (Fig. 4). We believe that the modification of Si and/or the formation of Si twinning can be attributed to at least two factors. One factor is the cooling rate. Higher cooling rates (i.e. melt spun Al–5Si alloys) promote Si twinning (Figs. 9 and 10).[13] Lower cooling rates (i.e. thermal analysis, 22 K min^{-1}) reduce or lose the possibility of Si twinning. The other factor is the distribution of the modified element. The Sr enrichment at the re-entrant edges/or corner of the eutectic Si promotes the Si twinning on the grain boundary.[9,10,19] It is also true for the Eu element.[11] This enrichment of Sr and Eu at the re-entrant edges/or corner of the eutectic Si was believed to be attributed to the modification effects from coarse and flake-like to fine and fibrous morphology. In contrast, the Y atom is likely to precipitate as AlY and/or Al_2SiY phase rather than concentrate within the eutectic Si (Fig. 12*c*). The absence of the Y element within the eutectic Si may partly explain why no significant Si twinning was observed in alloy B with 200 ppm Y addition, even through Y has a suitable radius ratio (r_Y/r_{Si}=1·459) according to the IIT theory and a large negative mixing enthalpy.

In contrast to conventional casting, some refiner multiply twinned Si particles were observed in high purity melt spun Al–5Si–200 ppm Y alloy. A higher cooing rate (i.e. 10^6 K s^{-1}, melt spinning) may extend the solid solubility of Y in the α-Al matrix.[29] More Y was dissolved into the α-Al matrix. This can partly explain why the AlY phase was observed in Al–5Si–200 ppm Y alloys (alloys B and D) produced by conventional casting, while no similar Y containing particles were observed in high purity melt spun Al–5Si–200 ppm Y alloys (alloy F). The higher solid solubility of Y in Al or Si can be expected to result in a redistribution of Y element and thus Si twinning, as shown in Fig. 9. In the annealed state, almost all Y precipitates form intermetallic compounds, as shown in Figs. 11 and 12. However, a very small amount of Y may be still retained in the lattice, resulting in Si twinning, as shown in Fig. 10. All these results strongly suggest that the partition behaviour of modified elements is of great importance to Si twinning and thus the modification effect on eutectic Si. This suggestion is also consistent with the previous report in Ref. 30, where the addition of Sr was reported to significantly alter the liquid structure of Al–Si alloys, which leads to changes in fundamental physical properties (i.e. rheological properties, specially the melt viscosity, interface energy of the interdendritic liquid during the final stages of solidification) of the alloy liquid, and thus delay or inhibit the clustering tendencies of the atoms at temperatures near the nucleation event. Similarly, the addition of Y can be also expected to change the atomic structure of Al–Si eutectic melt, delay the nucleation event of the eutectic Si and thus lead to a significant undercooling (Figs. 1 and 6). This is especially true for the case of high purity melt spun Al–Si alloys (alloys E and F). Higher cooling rates greatly refine the eutectic Si structure and extent the solid solubility of Y in Al or Si. Supersaturating environments of Si and Y can be achieved in the interdendritic liquid during solidification. In the annealed condition, Y containing phase was favourable to form in the interdendritic environment. This may explain why the Al_2SiY phase was formed beside the eutectic Si (Fig. 11) or within the Si particle (Fig. 12). Furthermore, research on the liquid structure of Al–Si–Y alloy is required.

Last, but definitely not least, we would like to point out that the maximum solubility of the rare earth in Al alloy is very small. In the case of Al–Y binary alloy, the maximum solubility is only 0·17 wt-% (0·05 at-%) at 912 K and becomes negligibly small at room temperature. During the solidification process, Y and Si elements were rejected to the front of the advancing solid/liquid interface. A constitutional undercooling was established, which restricts the growth of eutectic Si and thus refines the eutectic Si structure. This refinement mechanism caused by undercooling is different from the well known IIT and TPRE modification mechanisms, because, unlike Sr and Eu, Y does not greatly partition into the eutectic Si. Given the modification is mainly focused on the morphology change from plate-like to fibrous, we therefore prefer to describe the effect of Y as well as the other similar rare earth elements (i.e. Yb, Ce and Sc) on eutectic Si as a refinement rather than a modification.

Conclusions

A series of Al–5Si alloys with or without 200 ppm Y addition have been produced using conventional casting and melt spinning respectively. The effects of Y addition and cooling rates on the refinement of eutectic Si have been investigated using thermal analysis, DSC and multiscale microstructure characterisation techniques. In the case of conventional casting, the addition of 200 ppm Y into Al–5Si alloy was found to cause a refined plate-like structure rather than a fibrous morphology. No significant Si twinning was observed. In the case of melt spinning, a higher cooling rate caused a much finer eutectic Si and Si twinning. The addition of 200 ppm Y promoted a heavier multiply Si twinning. Furthermore, after a continuous cooling from 873 to 673 K, an Al_2SiY phase was observed beside or within the Si particle. This investigation highlights the

importance of the partition behaviour of the modified agents when discussing the refinement or modification mechanism.

Acknowledgement

J. H. Li gratefully acknowledges Professor G. Dehm for his access to TEM at the Erich Schmid Institute of Materials Science of the Austrian Academy of Science.

References

1. A. Pacz: Alloy. US Patent 1387900, 1921.
2. S.-Z. Lu and A. Hellawell: *Metall. Trans. A*, 1987, **18A**, 1721–1733.
3. B. Li, H. W. Wang, J. C. Jie and Z. J. Wei: *J. Alloys Compd*, 2011, **509**, 3387–3392.
4. K. Nogita, A. Knuutinen, S. D. McDonald and A. K. Dahle: *J. Light Met.*, 2001, **1**, 219–228.
5. A. Knuutinen, K. Nogita, S. D. McDonald and A. K. Dahle: *J. Light Met.*, 2001, **1**, 229–240.
6. W. Prukkanon, N. Srisukhumbowornchai and C. Limmaneevichitr: *J. Alloys Compd*, 2009, **477**, 454–460.
7. Y. C. Tsai, C. Y. Chou, R. R. Jeng, S. L. Lee and C. K. Lin: *Int. J. Cast Met. Res.*, 2011, **24**, 83–87.
8. Q. Y. Zhang, C. G. Zheng and W. S. Han: *Acta Metall. Sin.*, 1981, **17**, 130–136.
9. M. Timpel, N. Wanderka, R. Schlesiger, T. Yamamoto, N. Lazarev, D. Isheim, G. Schmitz, S. Matsumura and J. Banhart: *Acta Mater.*, 2012, **60**, 3920–3928.
10. K. Nogita, H. Yasuda, K. Yoshida, K. Uesugi, A. Takeuchi, Y. Suzuki and A. K. Dahle: *Scr. Mater.*, 2006, **55**, 787–790.
11. K. Nogita, H. Yasuda, M. Yoshiya, S. D. McDonald, K. Uesugi, A. Takeuchi and Y. Suzuki: *J. Alloys Compd*, 2010, **489**, 415–420.
12. M. Faraji and L. Katgerman: *Micron*, 2010, **41**, 554–559.
13. M. Zarif, B. McKay and P. Schumacher: *Metall. Mater. Trans. A*, 2011, **42A**, 1684–1691.
14. X. Jian, T. T. Meek and Q. Han: *Scr. Mater.*, 2006, **64**, 893–896.
15. J. B. Yu, Z. M. Ren and K. Deng: *Acta Metall. Sin.*, 2011, **24**, 301–308.
16. E. A. Brandes and C. J. Smithells: 'Metals reference handbook', 6th edn, 6–29; 1983, London, Butterworth Publishing Company.
17. B. Cantor: *Mater. Sci. Eng. A*, 1997, **A226–A228**, 151–156.
18. T. Dagerhamn: *Acta Chem. Scand.*, 1963, **17**, 267.
19. Y. K. Lee, N. Fujimura, N. Nishida and T. Ito: 'Polycrystalline semiconductors II', in 'Springer proceedings in physics', (ed. J. H. Werner and H. P. Strunk), Vol. 54; 1991, Heidelberg/Berlin, Springer-Verlag.
20. P. Villars and Calvert (eds.): 'Pearsons handbook of crystallographic data of intermetalic phase', Vols. 1–3, 3258; 1985, Materials Park, OH, American Society for Metals.
21. D. Turnbull and B. Vonnegut: *Ind. Eng. Chem.*, 1952, **44**, 1292.
22. M. E. Schlesinger: *Chem. Rev.*, 2002, **102**, 4267.
23. C. R. Ho and B. Cantor: *J. Mater. Sci*., 1995, **20**, 1912.
24. J. H. Li, M. Zarif, G. Dehm and P. Schumacher: *Philos. Mag*., DOI:10.1080/14786435.2012.687840.
25. O. Knacke, O. Kubaschewski and K. Hesselmann: *J. Phys. Chem. Ref. Data*, 1982, **11**, 2.
26. R. S. Wanger: *Acta Metall.*, 1960, **8**, 57.
27. R. D. Hamilton and R. G. Seidensticker: *J. Appl. Phys.*, 1960, **31**, 1165.
28. H. S. Kang, W. Y. Yoon, K. H. Kim, M. H. Kim, Y. P. Yoon and I. S. Cho: *Mater. Sci. Eng. A*, 2007, **A449–A451**, 334–337.
29. M. E. van Dalen, R. A. Karnesky, J. R. Cabotaje, D. C. Dunand and D. N. Seidman: *Acta Mater.*, 2009, **57**, 4081–4089.
30. P. Srirangam, M. J. Kramer and S. Shankar: *Acta Mater.*, 2011, **59**, 503–513.